Published in final edited form as:
Nat Neurosci. 2013 September ; 16(9): . doi:10.1038/nn.3473.

TARP γ-7 selectively enhances synaptic expression of calcium-permeable AMPARs

Dorota Studniarczyk, **Ian Coombs**, **Stuart G. Cull-Candy**, and **Mark Farrant**
Department of Neuroscience, Physiology and Pharmacology, University College London, Gower Street, London WC1E 6BT, UK

Summary

Regulation of calcium-permeable AMPA receptors (CP-AMPARs) is critical in normal synaptic function and neurological disease states. While transmembrane AMPAR regulatory proteins (TARPs) such as stargazin (γ-2) modulate the properties of calcium-impermeable (CI-) AMPARs and promote their synaptic targeting, the TARP-specific rules governing CP-AMPAR synaptic trafficking remain unclear. We used RNA interference to manipulate AMPAR subunit- and TARP expression in γ-2-lacking *stargazer* cerebellar granule cells – the classic model of TARP deficiency. We found that TARP γ-7 selectively enhanced synaptic expression of CP-AMPARs and suppressed CI-AMPARs, identifying a pivotal role of γ-7 in regulating the prevalence of CP-AMPARs. In the absence of associated TARPs, although their properties were altered, both CP- and CI-AMPARs were able to localize at synapses and mediate transmission. Finally, our results establish that TARPed synaptic receptors in granule cells require both γ-2 and γ-7, and reveal an unexpected basis for the loss of AMPAR-mediated transmission in *stargazer* mice.

Introduction

AMPA-type glutamate receptors mediate fast excitatory synaptic transmission in the CNS[1] and can be either calcium-impermeable or calcium-permeable (CI- or CP-AMPARs). The dynamic regulation of the CP-AMPAR subtype appears critical both in normal excitatory synaptic function and various debilitating neurological conditions[2-5]. The key determinant of AMPAR calcium permeability is RNA editing at the Q/R site in the pore-lining region of the GluA2 subunit[6,7]. Receptors that lack GluA2 display a number of functionally important properties: not only are they permeable to calcium ions[8-10], they also exhibit a high single-channel conductance compared with their edited counterparts, and are blocked by endogenous intracellular polyamines, giving rise to inwardly rectifying currents[11-13]. These various features are important in defining basic properties of excitatory transmission at synapses expressing CP-AMPARs[14,15], which can be rapidly modified by the differential removal or insertion of this AMPAR subtype[16,17]. Although there is considerable evidence that GluA2-containing- (CI-) and GluA2-lacking CP-AMPARs can be independently regulated and trafficked within individual neurons[11-13,18] the role played by auxiliary AMPAR subunits, in this process, remains unclear. In particular, no specific auxiliary subunits have yet been established to selectively regulate neuronal CP-AMPARs.

Transmembrane AMPAR regulatory proteins (TARPs) have emerged as key molecular determinants of native AMPAR behavior[19-24]. Multiple TARP family members have been

Authors for correspondence MF: m.farrant@ucl.ac.uk SGC-C: s.cull-candy@ucl.ac.uk.
Author Contributions S.G.C-C. and M.F. conceived and supervised the project. D.S. performed electrophysiological and biochemical experiments. M.F. and D.S analyzed the data. I.C. generated reagents for RNA interference and performed biochemical experiments. D.S., S.G.C-C. and M.F. wrote the manuscript.

Europe PMC Funders Author Manuscripts

described – γ-2, γ-3, γ-4, γ-8 (Ref. [25]) together with the homologous proteins γ-5 and γ-7 (Refs [26],[27]). Each of these TARPs exhibits a unique pattern of expression in the central nervous system[28,29]. Previous work has suggested that γ-5 selectively influences the functional properties of long-form CP-AMPAR subunits[27], but in the cerebellum this TARP is restricted to Bergmann glia[28], raising the question of whether another TARP (or TARPs) may serve a similar role within neurons. In this regard, two recent studies have addressed the involvement of γ-2 in synaptic localization of CP-AMPARs in cerebellar stellate cells. These have variously proposed, either that γ-2 is required for the normal synaptic localization of both CP-and CI-AMPARs subtypes[30], or alternatively that γ-2 is required for the synaptic expression of CI-AMPARs while under certain conditions CP-AMPARs can localize at synapses in the absence of γ-2, even though 'TARPless'[31]. Thus, the TARP-specific rules governing synaptic targeting of CP-AMPARs are currently unresolved.

The pivotal role of TARPs in the regulation and delivery of synaptic AMPARs emerged from experiments on cerebellar granule cells. The prototypical TARP stargazin (γ-2) is lost in the naturally occurring ataxic mutant mouse *stargazer*, where deficits in cerebellar function have been attributed to a specific lack of AMPARs at the granule cell surface and a selective loss of AMPAR-mediated EPSCs at the mossy fiber-granule cell synapse[32,33]. While this selective defect in *stargazer* mice was ascribed to the loss of the sole TARP in granule cells[25], it is now clear that γ-7, which is present in granule cells and other cerebellar neurons[28,29], can also act as a TARP[26]. Unlike other TARPs, γ-7 and γ-5 possess unusually short C-tails that lack the TTPV motif critical in the binding of TARP-associated AMPARs to PSD-95 and in clustering at the synapse[34]. Our recent work has suggested that γ-7 can associate with extrasynaptic CP-AMPARs but is not present at the synapse in *stargazer* stellate cells[31].

Granule cells express a limited repertoire of AMPAR subunits – predominantly the short-forms of GluA2 and GluA4[35-37]. In addition, they lack cornichons, which function as auxiliary AMPAR subunits in certain neurons[38,39]. Thus, granule cells provide a well-defined system in which to address the issue of TARP selectivity in the regulation of CP- and CI-AMPAR subtypes. We examined properties of AMPAR-channels in granule cells from *stg/stg* and wild-type mice, in which TARP- and GluA2 expression were modified through overexpression or knockdown by RNA interference. Our results demonstrate that in granule cells, CP- and CI-AMPARs are both capable of mediating synaptic transmission in the absence of an associated TARP. Furthermore, by providing evidence that TARP γ-7 selectively enhances synaptic expression of CP-AMPARs and suppresses CI-AMPARs, we have established that TARP γ-7 plays a key role in regulating the presence of neuronal CP-AMPARs at synapses. Our results also reveal an unexpected basis for the loss of surface AMPARs in *stargazer* granule cells.

Results

CP-AMPARs in granule cells after siRNA GluA2 knockdown

To examine the regulation of CP-AMPARs, and their interaction with TARPs, we transfected cerebellar granule cells with small interfering RNAs (siRNAs) designed to disrupt GluA2 production (see **Methods**). Initially, we compared the rectification properties of AMPAR currents by examining whole-cell responses to bath-applied AMPA (20 μM) during voltage-ramps (−90 to +60 mV) in untreated (wild-type; 'WT control') and transfected ('WT ΔGluA2') cells with an 'intracellular' solution containing added spermine. Untreated granule cells generated linear current-voltage (I-V) plots characteristic of GluA2-containing receptors. These gave a rectification index (see **Methods**) of 1.00 ± 0.09 (n = 17) (Fig. 1a). In contrast, transfected cells exhibited inwardly rectifying I-V plots, reflecting voltage-dependent block of GluA2-lacking CP-AMPARs by spermine (Fig. 1a). The

rectification index in transfected cells was significantly reduced compared with control cells (0.18 ± 0.06, $n = 6$; $P = 3.2 \times 10^{-6}$, see **Methods**) (Fig. 1b) (Supplementary Table 1 and 2). This pronounced increase in rectification was not caused by the transfection procedure itself, as cells transfected with GFP alone displayed I-V plots indistinguishable from control (rectification index = 0.81 ± 0.10, $n = 10$; $P = 1.00$) (Fig. 1b).

It is of note that the incomplete spermine block observed at positive potentials in transfected cells (Fig. 1a) would be expected for γ-2 associated CP-AMPARs[40]. Indeed, the action of 1-naphthyl acetyl spermine (NASPM), which produces a preferential voltage- and use-dependent block of CP-AMPAR channels when applied from the extracellular side of the membrane[41,42], was consistent with effective GluA2 knockdown. Thus, in transfected cells, bath applied NASPM (100 μM) produced an almost complete block of the AMPA-evoked current at −60 mV (Fig. 1c), suggesting that a majority of AMPARs were calcium-permeable following siRNA transfection. NASPM block was significantly greater in treated- compared with untreated cells ($n = 6$ in each condition; $P = 1.73 \times 10^{-4}$) (Fig. 1d). While NASPM produced ~40% block in untreated cells, the effect was not voltage-dependent (Fig. 1d), consistent with the view that it also produces some non-specific block of CI-AMPARs[43]. We obtained qualitatively similar results using a lower concentration of NASPM (3 μM): 18.0 ± 5.6 % block in control *versus* 51.2 ± 4.7 % block following knockdown ($n = 5$ and 4; $P = 0.016$).

Do CP-AMPARs in ΔGluA2 granule cells display other properties indicative of TARP association? We have previously shown that the single-channel conductance of CP-AMPARs is considerably higher than that of their calcium-impermeable counterparts, and that association with γ-2 typically enhances their conductance by a further 40% (Ref. [40]). Furthermore, it has also been demonstrated that TARP association shifts the proportion of openings towards the larger of four open levels displayed by these multi-conductance channels, and significantly enhances their burst duration[44]. To estimate the conductance of extrasynaptic AMPAR channels we used non-stationary fluctuation analysis (NSFA, see **Methods**) of responses activated by rapid application of 1 mM AMPA onto outside-out membrane patches (Fig. 1e, f). Knockdown of GluA2 caused a marked increase in single-channel conductance (from 9.2 ± 0.8 pS to 34.0 ± 3.1 pS, $n = 7$ and 4, respectively; $P = 0.0060$) (Fig. 1f, g), which is consistent with the presence of TARPed CP-AMPARs [40,44].

In patches from ΔGluA2 cells that exhibited a sufficiently low noise level we observed single-channel openings in the tail of the macroscopic currents (Fig. 1e). All-point amplitude histograms of selected events (see **Methods**) gave a mean single-channel conductance of 43.0 ± 1.1 pS ($n = 11$) (Fig. 1h). These, long-lived, large-conductance bursts of openings, characteristic of receptors co-assembled with TARPs[20, 27, 31, 40], were evident only following knockdown of GluA2. The ~25% larger conductance estimate obtained from directly resolved channel openings (compared with NSFA) likely reflects bias toward the selection of long-lived openings. It is of note that any brief openings from CI-AMPARs, if present, would have contributed to the weighted-mean conductance estimated from fluctuation analysis[31]. Interestingly, the increase in whole-cell current (at −90 mV) from 148 ± 37 pA to 773 ± 210 pA ($n = 17$ and 6, respectively; Supplementary Table 2), is consistent with the marked increase in single-channel conductance that we observed following GluA2 knockdown. While our single-channel analysis allows us to identify the presence of TARPed receptors it does not permit quantitative conclusions about the *proportion* of receptors that contain TARPs.

Synaptic CP-AMPARs following knockdown of GluA2

Are CP-AMPARs present in the synaptic membrane following GluA2 knockdown, and are these associated with γ-2? In the presence of TTX miniature EPSCs (mEPSCs) were readily

detected (Fig. 2a). While their amplitudes were similar at −60 and +60 mV in control cells (rectification index 0.91 ± 0.08, *n* = 9), pronounced inward rectification was seen in GluA2-lacking cells (rectification index 0.35 ± 0.06, *n* = 12) (Fig. 2b) (Supplementary Table 3), with an associated doubling in mEPSC amplitude at −60 mV (from 22.1 ± 3.4 pA to 46.4 ± 7.9 pA; *P* = 0.0056).

To estimate the relative proportion of CP-AMPARs across synapses we also calculated the rectification index as the ratio of summed mEPSC peak conductances from records of equal duration at +60 mV and −60 mV[31]. This method takes into account the full range of possible behaviors at individual synapses, including those where currents might not be detected at +60 mV due to complete block by spermine (rectification index of 0). This approach also indicated a marked increase in rectification in ΔGluA2 cells (rectification index shifted from 0.88 ± 0.11 to 0.19 ± 0.05). The similar outcome from the two methods of analysis suggested that in granule cells, unlike cerebellar stellate cells[31], synapses were relatively homogeneous in their AMPAR content, and following GluA2 knockdown there were none where a substantial proportion of the current was carried by CI-AMPARs.

We next used peak-scaled NSFA (psNSFA, see **Methods**) to determine the weighted mean single-channel conductance of postsynaptic AMPARs (Fig. 2c). As expected, in ΔGluA2 cells there was a marked increase in the synaptic channel conductance (from 13.9 ± 1. 2 pS to 22.2 ± 2.2 pS, *n* = 13 and 17, respectively; *P* = 0.014) (Fig. 2d) (Supplementary Table 3 and 4), consistent with a preponderance of CP-AMPARs in the postsynaptic membrane. The difference in synaptic channel behavior between control and GluA2-lacking granule cells (expressing predominantly CI- and CP-AMPARs, respectively) was also clear when we plotted rectification index against conductance (Fig. 2e) (see also Supplementary Fig. 2). The relatively large single-channel conductance of synaptic receptors in GluA2-lacking granule cells suggests that, like the extrasynaptic CP-AMPARs, the synaptic CP-AMPARs were TARPed.

Synaptic localization of CP-AMPARs does not require γ-2

We next turned to *stargazer* (*stg/stg*) mice which lack γ-2, the predominant TARP in granule cells. In line with the consensus that γ-2 is required for the normal surface expression of AMPARs in these cells[20,32], bath application of AMPA (20 μM) produced virtually no detectable current (*n* = 8) (Fig. 3a). As untreated granule cells expressed only CI-AMPARs (Fig. 1 and Fig. 2), we asked whether the requirement for γ-2 was specific to CI-AMPARs. Remarkably, simple knockdown of GluA2 with siRNA restored AMPA responses in *stg/stg* granule cells (322.9 ± 40.4 pA at −90 mV, *n* = 5) (Fig. 3a). In this condition the currents displayed marked inward rectification, with a mean rectification index of 0.20 ± 0.04 (*n* = 5) (Fig. 3b). This result clearly demonstrates that γ-2 is not an absolute requirement for the expression of CP-AMPARs at the surface of granule cells.

The selective loss of AMPARs from granule cells in *stg/stg* mice is generally thought to reflect the critical role played by γ-2 in these cells, whereas many other neurons express additional TARP isoforms that impart a measure of redundancy[45]. While this might suggest that the CP-AMPARs present in *stg/stg* granule cells lacking GluA2 would be TARPless, there is compelling evidence that γ-7 is also expressed in these cells[26,28,29]. Therefore, to determine whether the extrasynaptic CP-AMPARs were associated with γ-7, we recorded macroscopic currents from outside-out somatic membrane patches and estimated the channel conductance, as described above for wild-type cells (Fig. 1). We readily detected AMPAR-mediated currents in patches from *stg/stg* ΔGluA2 granule cells (−17.9 ± 5.6 pA at −60 mV, *n* = 8 patches) (Fig. 3c). The weighted mean single-channel conductance obtained from NSFA was 22.3 ± 2.4 pS (*n* = 7) (Fig. 3d, e); this is lower than the NSFA conductance

estimate from WT ΔGluA2 cells (Supplementary Table 1 and 2), suggesting that in *stg/stg* ΔGluA2 cells there may be a mixture of TARPed and TARPless receptors[31].

In *stg/stg* ΔGluA2, we observed long-lived large single-channel openings in the tail of macroscopic currents; these gave a mean single-channel conductance of 39.7 ± 2.4 pS (n = 9) (Fig. 3c, e), indicative of TARPed CP-AMPARs. However, as seen with wild-type GluA2-lacking granule cells, the single-channel conductance from resolved events was larger than that estimated from NSFA, likely reflecting the presence of a small population of lower conductance channels that were too brief or small to be directly resolved. Importantly, the conductance of the directly resolved channels was not significantly different from that obtained in WT ΔGluA2 cells (Fig. 1h) (43.0 ± 1.1pS, P = 0.23), again suggesting that a significant proportion of extrasynaptic AMPARs were associated with a TARP – in this case γ-7 rather than γ-2. Additionally, the whole-cell I-V plots were similar in wild-type ΔGluA2 and *stg/stg* ΔGluA2 cells, as expected if the extrasynaptic CP-AMPARs were TARPed in both conditions (compare Fig. 3b with Fig. 1a). It is of note that this situation resembles that previously described in *stg/stg* cerebellar stellate cells[31], where extrasynaptic CP-AMPAR channels also exhibit properties indicative of co-assembly with γ-7.

We next asked whether γ-2 is necessary for the accumulation of CP-AMPARs at postsynaptic sites. Following GluA2 knockdown we detected mEPSCs in *stg/stg* granule cells (Fig. 3f). This clearly demonstrates that γ-2 is not required for synaptic targeting of these receptors. However, the lack of detectable mEPSCs at +60 mV suggests not only that the expressed synaptic AMPARs were calcium-permeable but also that they showed an unusually high sensitivity to block by intracellular polyamines, as might be expected if they were TARPless[31]. Consistent with this view, the weighted mean single-channel conductance of the synaptic receptors, estimated from psNSFA, was only 13.5 ± 0.9 pS (n = 7) (Fig. 3g, h), significantly less than that of synaptic CP-AMPARs in GluA2-lacking wild-type granule cells (P = 0.0093). Therefore, unlike CI-AMPARs, CP-AMPARs do not require γ-2 in order to form functional synaptic receptors in granule cells, and appear capable of doing so in the absence of an associated TARP.

AMPAR surface expression does not require associated γ-7

To establish more clearly the role of γ-7 in the expression of both CI- and CP-AMPARs in granule cells, we next used shRNA to knock down this TARP (see **Methods**). In wild-type granule cells, this led to an increase in the mean whole-cell AMPA-evoked current (Fig. 4a, b) (Supplementary Table 1 and 2); the I-V relationship remained essentially linear (Fig. 4c, d). These observations suggest that in the continued presence of γ-2, knockdown of γ-7 increases either the number of AMPAR channels, their single-channel conductance, or their open probability. In granule cells, therefore, γ-7 appears to suppress CI-AMPAR function. We next considered whether such suppression by γ-7 contributes to the lack of surface AMPARs in *stg/stg* granule cells (see Fig. 3a). Knockdown of γ-7 in *stg/stg* cells rescued AMPAR expression, yielding large whole-cell currents. However, unlike the whole-cell currents rescued by knockdown of GluA2 (see Fig. 3b), the I-V relationships displayed very little rectification, indicating the currents arose predominantly from CI-AMPARs (Fig. 4 e-h).

The fact that CI-AMPARs are expressed at the granule cell surface in *stg/stg* cells when γ-7 is knocked down reinforces the view that γ-7 may normally act to suppress surface expression of CI-AMPARs. Furthermore, when we knocked down both GluA2 and γ-7 in *stg/stg* granule cells, AMPAR-mediated currents could still be readily elicited (270.5 ± 95.5 pA at −90 mV; n = 7). These showed strong inward rectification (rectification index 0.28 ± 0.06), indicative of CP-AMPARs. Together these data suggest that, under appropriate

conditions, both CP- and CI-AMPARs may be expressed at the granule cell surface in the absence of an associated TARP.

Role of γ-7 in the delivery of synaptic AMPARs

The present data, and previous experiments on cerebellar stellate cells[31], support the idea that in *stg/stg* cells, extrasynaptic CP-AMPARs are associated with γ-7, while synaptic CP-AMPARs behave as if TARPless. As granule cells in *stg/stg* mice lack synaptic currents, despite the presence of γ-7, this raises the question of whether γ-7 normally plays any role in the regulation or synaptic localization of CI-AMPARs. Following γ-7 knockdown in wild-type granule cells we still detected mEPSCs (Fig. 5a), suggesting that CI-AMPARs can reach the synapse in the absence of this TARP. However, there was a clear decrease in synaptic channel conductance (to 8.9 ± 0.6 pS, $n = 9$; $P = 0.0093$) (Fig. 5a). Hence, while γ-7 is clearly not essential for synaptic localization it appears to play a role in regulating CI-AMPAR properties. The reduction in single-channel conductance suggests that, following knockdown of γ-7 the postsynaptic AMPARs may either be TARPless or composed of subunits (such as homomeric GluA2) that give rise to low conductance channels.

To determine whether γ-7 also plays a role in the regulation or synaptic clustering of CP-AMPARs, we examined mEPSCs in wild-type granule cells following the knockdown of both GluA2 and γ-7. When compared with cells in which only GluA2 had been knocked down, these cells displayed mEPSCs with reduced amplitudes and underlying synaptic channel conductances (both roughly halved; 14.5 ± 3.4 pA, $n = 10$ and 12.5 ± 0.8 pS, $n = 8$; $P = 0.049$ and 0.0036, respectively) (Fig. 5b). The reduction in amplitude and conductance cannot be attributed to the presence of CI-AMPARs, as mEPSCs remained strongly rectifying (Fig. 2b and Supplementary Table 3); instead the data suggest that synaptic CP-AMPARs are also TARPless following knockdown of γ-7. This also suggests a co-operative action of the two TARPs, with γ-2 unable to associate with synaptic receptors in the absence of γ-7.

We previously showed that in *stg/stg* granule cells synaptic currents are restored following knockdown of γ-7 (Ref. [31]). To determine whether the properties of the underlying receptors were changed, as might be expected for TARPless AMPARs, we recorded mEPSCs (at positive and negative voltages) from *stg/stg* granule cells with γ-7 knocked down (Fig. 5c) and performed psNSFA to estimate the underlying synaptic channel conductance. Although the mEPSCs displayed some inward rectification (Fig. 5c, d), the mean rectification index of 0.77 ± 0.09 ($n = 6$) suggested that CI-AMPARs contributed to a substantial proportion of the currents. This, and their low channel conductance (Supplementary Table 3 and 4) is consistent with the view that, like CP-AMPARs, these receptors can localize at the synapse in the absence of associated TARPs.

As we were able to rescue mEPSCs in *stg/stg* granule cells simply by disrupting GluA2 production, and rendering AMPARs calcium-permeable (see Fig. 3f), the suppressive action of endogenous γ-7 would appear selective for CI-AMPARs. Our experiments above suggest that synaptic CP-AMPARs in *stg/stg* mice are TARPless even in the presence of γ-7. We therefore next considered whether or not the presence of γ-7 *per se* was necessary for synaptic localization of CP-AMPARs. To address this we examined *stg/stg* granule cells in which both GluA2 and γ-7 were knocked down. We detected strongly rectifying mEPSCs (rectification index of 0.26 ± 0.06, $n = 15$) in these cells, suggesting that, in the absence of both γ-2 and γ-7, TARPless CP-AMPARs were capable of accumulating at synapses. Furthermore, although the mean amplitude of mEPSCs was slightly reduced (Supplementary Table 3 and 4), the single-channel conductance from psNSFA (13.1 ± 1.6 pS, $n = 11$) was not significantly different from the value obtained from GluA2-lacking *stg/stg* cells ($P = 1.00$) (Supplementary Fig. 1). This supports the idea that in the absence of γ-2 synaptic CP-

AMPARs are TARPless, even in the presence of γ-7. Thus, although the presence of γ-7 does not appear necessary for CP-AMPAR delivery to the synapse, by suppressing the synaptic targeting of CI-AMPARs while permitting delivery of their calcium permeable counterparts, TARP γ-7 selectively favors the synaptic targeting of CP-AMPARs.

Interaction of TARPs γ-2 and γ-7

We next used co-immunoprecipitation assays to examine the interaction between TARP γ-7 and AMPARs, and that between γ-7 and γ-2. Previous studies have been unclear with regard to a possible interaction between γ-7 and γ-2 (Refs [26],[46]). In cerebellar lysates from wild-type and *stg/stg* adult mice, we found that γ-7 interacted with both GluA2 and GluA4 (Fig. 6) (see **Methods**). Moreover, in wild-type samples γ-7 interacted with γ-2, and as would be expected this interaction was not detected in stg/*stg* samples.

These results suggest that individual receptors can bind both γ-2 and γ-7 within the same assembly. Together, our functional and biochemical data support the idea of a cooperative role of TARPs γ-2 and γ-7 in AMPAR regulation (Yamazaki et 2010).

Overexpression of γ-7 promotes delivery of CP-AMPARs

Our knockdown data suggests that γ-7 may promote the surface expression of CP-AMPARs. To test this idea we transfected wild-type granule cells with γ-7 cDNA. The overexpression of γ-7 increased the mean amplitude of whole-cell AMPAR-mediated currents by nearly an order of magnitude (Supplementary Table 1 and 2). These currents displayed strong inward rectification, indicating they were mediated predominantly by CP-AMPARs (Fig. 7a). To exclude the possibility that merely increasing the expression of any TARP could result in increased delivery of CP-AMPARs to the cell surface, we examined whole-cell responses in wild-type cells in which γ-2 was over-expressed. Whilst this treatment increased the whole-cell currents (Supplementary Table 1 and 2), they retained their linear I-V relationships (Fig. 7b and c), with a mean rectification index that was not different from that seen in untreated cells (Fig. 7d), but markedly different from that seen in γ-7 over-expressing cells. This confirmed that enhanced expression of TARPs *per se* did not result in an increased surface expression of CP-AMPARs.

Over-expression of γ-7 also resulted in a marked increase in the amplitude of mEPSCs (at −60 mV) (Fig. 7e and f), and a pronounced increase in inward rectification (Fig. 7f). Consistent with this being caused by increased synaptic expression of CP-AMPARs, the weighted mean conductance (estimated from psNSFA) of the underlying channels was almost doubled, to 20.3 ± 1.4 pS (n = 6; P = 0.025 *versus* wild-type granule cells) (Fig. 7f). Overall, the mEPSCs recorded after over-expression of γ-7 displayed properties similar to those mediated by CP-AMPARs following knockdown of GluA2 (see Fig. 2). These results are in accord with observations from knockout mice showing that the relative expression of TARPs γ-2 and γ-7 influences AMPAR subunit composition, leading to distinct changes in AMPAR subunit abundance in the whole cerebellum and changes in subunit labeling at mossy fiber-granule cell synapses[29]. Taken together, our data indicate that increased expression of γ-7 increases the prevalence of CP-AMPARs at synaptic and extrasynaptic sites. It is particularly striking that this can be induced in cells that do not normally express CP-AMPARs. Of note, following γ-7 over-expression synaptic CP-AMPARs exhibit properties which indicate they are TARPed. This differs from the situation in *stg/stg* granule cells lacking GluA2, where only the extrasynaptic AMPARs appeared to be TARPed. This presumably reflects the fact that granule cells from wild-type mice express γ-2, and is in keeping with our finding that the presence of both γ-2 and γ-7 is necessary and sufficient for synaptic CP-AMPARs to be TARPed in granule cells.

Discussion

Our results establish that TARP γ-7 plays an essential role in regulating the prevalence of neuronal CP-AMPARs. Specifically, γ-7 suppresses the surface expression of CI-AMPARs while promoting delivery of their calcium-permeable counterparts. Our experiments also indicate that γ-7 co-operates with γ-2 in the proper maintenance of AMPAR surface expression and synaptic targeting in cerebellar granule cells, such that knockdown of γ-7 leads to the expression TARPless synaptic CI-AMPARs. Furthermore, our findings provide a new explanation for the absence of AMPARs at granule cell synapses in *stg/stg* mice. This we ascribe to a suppressive action of γ-7 on the surface expression of CI-AMPARs, rather than a lack of functional TARPs.

CP-AMPARs can localize at synapses without associated TARP

The identification of TARPs arose from experiments examining the defect in mossy fiber-granule cell synaptic transmission in the mutant mouse *stargazer*. Thus, there has been great interest in the role played by TARPs in regulating the properties of AMPARs in these cells. Transfection with siRNA against GluA2 enabled us to influence AMPAR subunit composition in granule cells and address the TARP-specific regulation of synaptic CP-AMPARs.

The lack of synaptic AMPARs in granule cells of *stg/stg* mice has previously been interpreted in terms of a role of the predominant TARP γ-2. Our finding, that simple knockdown of GluA2 is sufficient to rescue excitatory transmission in *stg/stg* granule cells, unambiguously demonstrates that trafficking and clustering of CP-AMPARs to postsynaptic sites can occur without γ-2 and that the absence of synaptic AMPARs reflects the predominance of CI-AMPARs in these cells. Indeed, as transmission can also be rescued by γ-7 knockdown, it is clear that neither γ-2 nor γ-7 is essential for the synaptic targeting of either AMPAR subtype, and that TARPless CP- and CI-AMPARs are both capable of localizing at these synapses.

Both γ-2 and γ-7 are required for TARPed synaptic AMPARs

Although neither γ-2 nor γ-7 is required for the synaptic localization of CP- or CI-AMPAR subtypes, the presence of both is necessary for synaptic AMPARs to exhibit their normal functional properties. Thus, following knockdown of γ-7 alone, synaptic CI-AMPARs displayed a reduced channel conductance, similar to that seen when both TARPs were absent. Likewise, synaptic CP-AMPARs in ΔGluA2 cells lacking either TARP exhibited properties that resembled those seen when both TARPs were absent – namely an increased sensitivity to block by intracellular spermine and a reduced single-channel conductance. These observations suggest that both γ-2 and γ-7 are essential for synaptic AMPARs to be TARPed.

It is of particular interest that in *stg/stg* ΔGluA2 granule cells the resolved channel openings of extrasynaptic CP-AMPARs occurred as long-lived high-conductance bursts, characteristic of TARPed receptors[20, 40]. This, together with our co-immunoprecipitation data from *stg/stg* brain lysates, indicates that γ-2 is not required for TARP γ-7 to associate with AMPARs. However, the low single-channel conductance and pronounced inward rectification of the synaptic CP-AMPARs in these same cells suggest that the synaptic receptors are TARPless, and thus that there is compartment-specific regulation[31]. The absence of γ-7-associated CP-AMPARs from the synapse, despite their presence extracellularly, suggests either that they fail to cluster at synaptic sites, or are actively excluded from the sub-synaptic membrane, or that TARPless receptors are clustered preferentially.

Relatively few studies have addressed directly the question of how multiple TARP subtypes act in concert to control AMPAR expression, and thereby regulate excitatory synaptic transmission. Both γ-2 and γ-8 are known to be required for maintenance of normal AMPAR-mediated synaptic currents in hippocampal neurons[47], while γ-2 and γ-3 are both required for normal transmission in cerebellar Golgi cells[45]. A recent immunogold labeling study of AMPARs and TARPs at cerebellar synapses of knockout mice (lacking γ-2, γ-7, or both TARP subtypes) proposed that γ-2 and γ-7 might co-operate in promoting expression of synaptic AMPARs in the cerebellum[29]. Previous work has suggested that γ-2 and γ-7 might co-assemble (Kato et al 2007; 2008). Our co-immunoprecipitation data suggest that γ-2 and γ-7 co-operate to regulate synaptic transmission in cerebellar granule cells through co-assembly with the same receptors, rather than individually assembling in a competitive manner.

Dual action of TARP γ-7

In *stg/stg* granule cells, AMPARs fail to reach the surface membrane, even though GluA2 and GluA4 proteins are present intracellularly[25,32,33]. Together with the rescue of transmission following knockdown of GluA2, the fact that γ-7 knockdown restored the surface expression and synaptic targeting of CI-AMPARs strongly suggests that this intracellular retention results not from the lack of γ-2 *per se*, but rather from an AMPAR subtype-specific suppression by γ-7. Accordingly, in wild-type granule cells, knockdown of γ-7 increased the whole-cell current amplitude while maintaining the predominance of CI-AMPARs.

By contrast, overexpression of γ-7 in wild-type granule cells caused an increase in the AMPAR-mediated whole-cell current (at negative potentials) that was accompanied by a dramatic shift in the I-V relationship, from roughly linear to strongly inwardly rectifying, reflecting the insertion of CP-AMPARs. A similar change was observed with synaptic receptors – mEPSC amplitude, rectification and weighted mean synaptic channel conductance were all greatly enhanced by expression of γ-7. Thus, while loss of γ-7 enhanced the expression of GluA2-containing CI-AMPARs at the cell surface and resulted in potentially TARPless CI-AMPARs at the synapse, elevation of γ-7 enhanced the expression of GluA2-lacking CP-AMPARs and resulted in TARPed synaptic CP-AMPARs. Overall, γ-7 appears to reduce the prevalence of CI-AMPARs at both extrasynaptic and synaptic sites while promoting the expression of CP-AMPARs.

Our data show that the manipulation of either γ-2 or γ-7 expression in granule cells results in profound changes in AMPAR properties and suggests the following ‘rules’. TARP γ-7 association promotes surface delivery of CP-AMPARs, while it inhibits GluA2-containing receptors from reaching the cell surface. Its association with either CP- or CI- AMPARs inhibits their synaptic localization unless the assembly also contains γ-2. Thus, CI- and CP-AMPARs localize at these synapses only when TARPed with both γ-2 and γ-7, or if they are TARPless. Although AMPAR/TARP stoichiometry remains unresolved[48-50], our data indicate that γ-2 and γ-7 associate with the same assembly, tightly regulating normal AMPAR targeting.

Methods

Animals

Individual male and female C57BL/6 (‘WT’) and *stargazer* (‘*stg/stg*’) mice (postnatal day 4-7; P4-7) were used to prepare dissociated cultures of cerebellar granule cells. *Stargazer* mice were bred by crossing +/*stg* animals (C57BL/6 genetic background). Tail samples were used for genotyping to enable culture identification[51]. The primers used were

ETn-OR 5′ -GCCTTGATCAGAGTAACTGTC-3′

109F 5′ -CATTTCCTGTCTCATCCTTTG-3′

JS167 5′ -GAGCAAGCAGGTTTCAGGC-3′

E/Ht7 5′ -ACTGTCACTCTATCTGGAATC-3′

Cerebellar tissue for culture preparation was from animals selected only on the basis of age and geneotype (homozygous *stg/stg* or WT +/+). All procedures for the care and treatment of mice were in accordance with the U.K. Animals (Scientific Procedures) Act 1986.

Dissociated cultures

Briefly, after decapitation, the cerebella were removed, cut into small pieces and trypsinized at 37°C. Mechanically dissociated cells were plated on poly-L-lysinecoated (Sigma) glass coverslips, at a density of 2.1×10^5 cells per coverslip. Cells were maintained in a humidified atmosphere at 37 °C (5% CO_2) in Basal Medium Eagle (BME) supplemented with 10% fetal bovine serum (FCS; vol/vol), 2 mM L-glutamine and 100 mg ml^{-1} gentamicin (all Gibco). Cells were maintained in 'high K^+' (25 mM KCl) to promote synaptic maturation. Cytosine arabinoside (10 μM; Sigma) was added 24 h after plating to inhibit glial proliferation.

Transfection

For experiments requiring knock down or overexpression of AMPAR subunits or TARPs, cells were transfected after 3-10 days *in vitro*, using the calcium phosphate method. TARP γ-2 cDNA (rat) was a gift from R. Nicoll (UCSF). TARP γ-7 cDNA (human) was from OriGene Technologies Inc. Cultures transfected with γ-2 or γ-7 were treated with NBQX (50 μM) to prevent cell death. For knockdown of GluA2, siRNA corresponding to nucleotides 400-418 of mouse GluA2 (Ref.[52]) was incorporated into the U6 siStrike vector from Ambion, according to the manufacturer's instructions. Primers were from Sigma Genosys: Fwd – ACCGAGCACTCCTTAGCTTGATCTTCCTGTCAATCAAGCTAAGGAGTGCTCTTTTTC; Rvs – TGCAGAAAAAGAGCACTCCTTAGCTTGATTGACAGGAAGATCAAGCTAAGGAGTGCT. The vector contained the GFP reporter gene. siRNAs targeting the same nucleotides have been reported to produce a >90% loss of GluA2 (Ref. [52]). For knockdown of TARP γ-7, cells were transfected with a mixture of four shRNA expression constructs against γ-7 (GeneCopoeia MSH037278-mU6; 2 μg per coverslip). The target sequences were; mouse γ-7 (Accession No. NM 133189.3) 54 (5′-CTGCGGCCTGCTCCTTGTG-3′), 176 (5′-GGAGAGTCTGCTTCTTTGC-3′), 374 (5′-CTCAGAGGACCATTCTTGC-3′) and 500 (5′-CTGAGCAGTACTTTCACTA-3′). The constructs contained the mCherryFP reporter gene. Cells were typically transfected with 2 μg of the cDNA of interest. For experiments involving double knockdown, we used 2 μg siGluA2: 1 μg shγ-7. Recordings were made from un-transfected and transfected (red or green fluorescent) cells 2-4 days later.

Quantification of γ-7 shRNA efficiency and selectivity

Granule cell cultures prepared from P7 mice were transfected with γ-7 shRNA, as described above. After 2 days they were fixed for 10 min in a solution of 4% paraformaldehyde (TAAB labs) and 4% sucrose in PBS. Cells were then incubated in 50 mM NH_4Cl then blocked with 0.3% BSA (both in PBS) for 15 min each. Coverslips were incubated in blocking solution with anti-γ-7 antibody (rabbit, 7 μg/ml; a gift form Masahiko Watanabe, Department of Anatomy, Hokkaido University School of Medicine) for 30 min, washed three times then incubated with an Alexa 488 conjugated goat anti-rabbit secondary

antibody (Invitrogen) for a further 30 min. Following three further washes, coverslips were mounted on slides using Prolong Gold anti-fade mounting medium (Invitrogen) and imaged using a confocal microscope (Carl Zeiss LSM) using a 40× oil-immersion objective. We identified isolated cells successfully transfected with shRNA (expressing mCherryFP) and, for each cell, compared the mean florescence intensity of the somatic Alexa 488 signal with that of 4–8 untransfected cells in the same field of view. We made measurements from 10 fields using ImageJ [53]. Overall, γ-7 protein was depleted by 67 ± 6% in individual granule cells after transfection with the γ-7 shRNAs. This is likely to be a slight underestimate, as transfected cells expressing high levels of mCherryFP displayed some bleed-through into the Alexa488 signal, but is comparable to that seen in a previous study utilizing shRNA-induced knockdown of γ-7 (Ref. [54]).

The specificity of γ-7 shRNAs for γ-7 *versus* γ-2 was assessed by measuring current-voltage (I-V) relationships of whole-cell currents from tsA201 cells expressing recombinant homomeric GluA4 receptors with TARP γ-2 (Refs.[27,40]). Cells transfected with γ-7 shRNAs displayed I-Vs characteristic of γ-2 partial relief of spermine block [40]: rectification index (+60/−60mV) was 0.6, clearly different from that seen with GluA4 in the absence of γ-2 (0.05; Ref. [27]).

Electrophysiology

Cells were viewed using a fixed-stage microscope (Axioskop FS1, Zeiss) and perfused at a rate of 1.5–2 ml min^{-1}. The extracellular solution contained 145 mM NaCl, 2.5 mM KCl, 1 mM $CaCl_2$, 1 mM $MgCl_2$, 10 mM glucose and 10 mM HEPES (adjusted to pH 7.3 with NaOH). To block voltage-gated sodium channels, NMDA-, $GABA_A$- and glycine receptors, 1 μM tetrodotoxin (TTX), 20 μM D-AP5, 20 μM SR-95531 and 1 μM strychnine (Ascent Scientific) were added. When recording synaptic currents, to increase mEPSC frequency the cells were briefly exposed (2-3 min) to 200 μM $LaCl_3$ prior to data acquisition[55]. Pipettes for whole-cell and outside-out patch recording were pulled from thick-walled borosilicate glass (1.5 mm o.d., 0.86 mm i.d., Harvard Apparatus), coated with Sylgard resin (Dow Corning 184) and fire-polished to a final resistance of ~5-8 or ~8-10 MΩ, respectively. Pipettes were filled with a solution containing 145 mM CsCl, 2.5 mM NaCl, 1 mM Cs-EGTA, 4 mM MgATP and 10 mM HEPES (adjusted to pH 7.3 with CsOH). Spermine tetrahydrochloride (500 μM, Sigma) was added to the intracellular solution. Currents were recorded at 22–26 °C using an Axopatch 1D amplifier and acquired using pClamp10 and a Digidata 1200 interface (Molecular Devices). Series resistance (10-45 MΩ) and input capacitance (3–8 pF) were read directly from the amplifier settings used to minimize the current responses to 5 mV hyperpolarizing voltage steps.

Whole-cell currents

We generated current-voltage (I-V) relationships by ramping membrane potential from −90 to +60 mV in the presence of 20 μM s-AMPA and 10 μM cyclothiazide (Ascent Scientific). Records were filtered at 2 kHz and sampled at 5 kHz. The rectification index (RI) was calculated as the ratio of slope conductance in the positive (+20 to +40 mV) and negative (−40 to −20 mV) limbs of the I-V (Igor Pro 6.10 WaveMetrics Inc. with NeuroMatic 2.5, http://www.neuromatic.thinkrandom.com).

Excised somatic patches

We pulled outside-out patches from the soma of granule cells. Currents were filtered at 10 kHz and digitized at 50 kHz. Fast agonist application was achieved using a double-barreled application tool made from theta glass (2 mm o.d.; Hilgenberg GmbH) pulled to a tip opening of ~200 μm, and mounted on a piezoelectric translator (Physik Instrumente). To enable visualization of the solution interface and allow measurement of solution exchange at

the end of each recording (10-90% risetime 200-250 μs), we added 2.5 mg ml^{-1} sucrose to the agonist solution and diluted the control solution by 5%. To determine channel properties from macroscopic responses, s-AMPA (1 mM) was applied (100-ms duration, 0.83 Hz) and the ensemble variance of all successive pairs of current responses calculated. The single-channel current (*i*) and the total number of channels (*N*) were determined by plotting this ensemble variance (□^{2}) against mean current $\left(\bar{I}\right)$ and fitting with the equation:

$$\sigma^2 = i\,\bar{I} - \bar{I}^2/N + \sigma^2_{\mathrm{B}} \quad (1)$$

The weighted-mean single-channel conductance was calculated from the single-channel current and the holding potential. No correction for liquid junction potential was made. Large single-channel openings in the tail of macroscopic patch currents were analyzed from records digitally filtered at 4 kHz. Clear channel events (lasting longer than ~3 ms) were selected by eye. For each event an all-point amplitude histogram was generated and fit with two Gaussians to determine the amplitude of the single-channel current. In each case the mean amplitude was at least 3× the SD of the background noise (0.4 – 0.9 pA).

mEPSC analysis

For mEPSC recordings, the signal was filtered at 2 kHz and sampled at 20 kHz. We detected mEPSCs using amplitude threshold crossing[56], with the threshold (typically ~6 pA) set according to the baseline current variance. The rectification index was calculated by dividing the mean mEPSC peak conductance calculated using all events detected at +60 mV and a matching number of the largest events at −60 mV. In some cases, to estimate the relative proportion of CP-AMPARs across synapses we also calculated the rectification index as the ratio of summed mEPSC peak conductances from records of equal duration at +60 mV and −60 mV. This method takes into account the full range of possible rectification at individual synapses, including those where currents might not be detected at +60 mV due to complete block by spermine (rectification index of 0)[31]. When analyzing charge-transfer, any event with a distinct peak was included. When analyzing mEPSC amplitude, all events with a monotonic rise were included, irrespective of overlapping decays. Finally, for fluctuation anlaysis (see below) and kinetic analysis only events that exhibited a monotonic rise and an uncontaminated decay were included. Such events were aligned on their rising phase prior to averaging.

We used peak-scaled non-stationary fluctuation analysis (ps-NSFA) to estimate the weighted mean single-channel conductance of synaptic receptors[57]. Each mEPSC was divided into 30 bins of equal amplitude and, within each bin, the variance of the mEPSC about the scaled average was computed. The variance was plotted against the mean current value, and the weighted mean single-channel current was estimated by fitting the full parabolic relationship with the equation:

$$\sigma^2_{\mathrm{PS}} = i\,\bar{I} - \bar{I}^2/N_{\mathrm{p}} + \sigma^2_{\mathrm{B}} \quad (2)$$

where σ^2_{PS} is the peak-scaled variance, $\bar{I}$ is the mean current, *i* is the weighted mean single-channel current, N_{p} is the number of channels open at the peak of the EPSC, and σ^2_{B} is the background variance. The mean chord conductance for each cell was calculated assuming a reversal of 0 mV.

Europe PMC Funders Author Manuscripts

The decay of averaged EPSCs was described by one, or more often two exponential functions. When fitted with two exponentials, the weighted time constant of decay ($\tau_{w,\ decay}$) was calculated as the sum of the fast and slow time constants weighted by their fractional amplitudes.

Co-immunoprecipitation from brain lysates

Cerebella of adult mice were homogenized in buffer I (0.32 M sucrose, 3 mM HEPES-Na, 0.1 mg/ml phenylmethylsulfonyl fluoride (PMSF), pH 7.4) and centrifuged at 16000 g for 10 min at 4°C. The pellets were solubilized with buffer II (50 mM Tris-HCl, 0.5 % Triton X-100, 150 mM NaCl, 1 mM EDTA, 1 mM PMSF and Complete Protease Inhibitor Cocktail; Roche) for 1 h at 4 °C. After centrifugation at 38000 rpm for 40 min, the supernatant was collected and the protein concentration determined using a Bradford Assay. 2 mg of protein was used per IP. The lysate was incubated overnight at 4 °C with 2 mg of γ-7 antibody (rabbit, 600 μg/ml; a gift form Masahiko Watanabe, Department of Anatomy, Hokkaido University School of Medicine). The following day, Protein G-Sepharose (Sigma) was added and incubated for 1 h. The protein G pellet was washed five times in buffer II. Adherent proteins were eluted with 2× SDS sample buffer at 95 °C for 5 min. The proteins were transferred onto nitrocellulose and blotted with 2 μg of anti-GluA2 (mouse, 1 mg/ml; Millipore MAB397), anti-GluA4 (goat, 200 μg/ml; Santa Cruz sc-7614) and anti γ-2 (guinea pig, 700 μg/ml; a gift form Masahiko Watanabe).

Data presentation and statistical analysis

Summary data are presented in the text as mean ± standard error (s.e.m.) from *n* cells or patches. The data are displayed graphically as box plots, showing the median (bar), mean (cross), interquartile range (box), and 10%–90% range (whiskers), with superimposed data from individual cells or patches (open circles). Comparisons involving two data sets only were performed with a two-sided Welch two-sample *t*-test. Although presented as selected pairwise comparisons in the Figures, all analyses involving data from three or more groups were performed using one-way ANOVA (Welch's heteroscedastic *F*-test), followed by pairwise comparisons using two-sided Welch two-sample *t*-tests (with Holm's sequential Bonferroni correction for multiple comparisons). Differences were considered significant at $P < 0.05$. Equivalent results were obtained using robust statistical methods that reduce effects associated with non-normality, outliers or unequal variance – an omnibus test of the hypothesis of equal trimmed means, followed by percentile bootstrap pairwise tests using trimmed means[58] (http://r-forge.r-project.org/projects/wrs) (Supplementary Table 2 and 4). All statistical tests were performed using R (version 2.15.2, The R Foundation for Statistical Computing; http://www.R-project.org) and RStudio (version 0.97.248, RStudio, Inc.). No statistical test was used to predetermine sample size and no randomization or blinding was employed. Hierarchical cluster analysis was performed using the DIvisive ANAlysis Clustering algorithm ('diana') in the R package 'cluster'[59] and grouping was identified using 'cutree'.

Supplementary Material

Refer to Web version on PubMed Central for supplementary material.

Acknowledgments

This work was supported by Programme Grants from the Wellcome Trust and the MRC (S.G.C.-C. and M.F.). We thank Cécile Bats for invaluable discussions and Marzieh Zonouzi and Masahiko Watanabe for advice on co-immunoprecipitation.

Europe PMC Funders Author Manuscripts

References

1. Traynelis SF, et al. Glutamate receptor ion channels: structure, regulation, and function. Pharmacol Rev. 2010; 62:405–496. [PubMed: 20716669]
2. Kuner R, et al. Late-onset motoneuron disease caused by a functionally modified AMPA receptor subunit. Proceedings of the National Academy of Sciences of the United States of America. 2005; 102:5826–5831. [PubMed: 15827116]
3. Liu B, et al. Ischemic insults direct glutamate receptor subunit 2-lacking AMPA receptors to synaptic sites. J Neurosci. 2006; 26:5309–5319. [PubMed: 16707783]
4. Park JS, et al. Persistent inflammation induces GluR2 internalization via NMDA receptor-triggered PKC activation in dorsal horn neurons. J Neurosci. 2009; 29:3206–3219. [PubMed: 19279258]
5. Gangadharan V, et al. Peripheral calcium-permeable AMPA receptors regulate chronic inflammatory pain in mice. J Clin Invest. 2011; 121:1608–1623. [PubMed: 21383497]
6. Sommer B, Kohler M, Sprengel R, Seeburg PH. RNA editing in brain controls a determinant of ion flow in glutamate-gated channels. Cell. 1991; 67:11–19. [PubMed: 1717158]
7. Rosenthal JJ, Seeburg PH. A-to-I RNA editing: effects on proteins key to neural excitability. Neuron. 2012; 74:432–439. [PubMed: 22578495]
8. Hollmann M, Hartley M, Heinemann S. Ca^{2+} permeability of KA-AMPA–gated glutamate receptor channels depends on subunit composition. Science. 1991; 252:851–853. [PubMed: 1709304]
9. Burnashev N, Monyer H, Seeburg PH, Sakmann B. Divalent ion permeability of AMPA receptor channels is dominated by the edited form of a single subunit. Neuron. 1992; 8:189–198. [PubMed: 1370372]
10. Geiger JR, et al. Relative abundance of subunit mRNAs determines gating and Ca^{2+} permeability of AMPA receptors in principal neurons and interneurons in rat CNS. Neuron. 1995; 15:193–204. [PubMed: 7619522]
11. Cull-Candy S, Kelly L, Farrant M. Regulation of Ca^{2+}-permeable AMPA receptors: synaptic plasticity and beyond. Current Opinion in Neurobiology. 2006; 16:288–297. [PubMed: 16713244]
12. Isaac JT, Ashby M, McBain CJ. The role of the GluR2 subunit in AMPA receptor function and synaptic plasticity. Neuron. 2007; 54:859–871. [PubMed: 17582328]
13. Liu SJ, Zukin RS. Ca^{2+}-permeable AMPA receptors in synaptic plasticity and neuronal death. Trends in Neurosciences. 2007; 30:126–134. [PubMed: 17275103]
14. Bowie D, Lange GD, Mayer ML. Activity-dependent modulation of glutamate receptors by polyamines. J Neurosci. 1998; 18:8175–8185. [PubMed: 9763464]
15. Rozov A, Burnashev N. Polyamine-dependent facilitation of postsynaptic AMPA receptors counteracts paired-pulse depression. Nature. 1999; 401:594–598. [PubMed: 10524627]
16. Liu SQJ, Cull-Candy SG. Synaptic activity at calcium-permeable AMPA receptors induces a switch in receptor subtype. Nature. 2000; 405:454–458. [PubMed: 10839540]
17. Gardner SM, et al. Calcium-permeable AMPA receptor plasticity is mediated by subunit-specific interactions with PICK1 and NSF. Neuron. 2005; 45:903–915. [PubMed: 15797551]
18. Man HY. GluA2-lacking, calcium-permeable AMPA receptors – inducers of plasticity? Current Opinion in Neurobiology. 2011; 21:291–298. [PubMed: 21295464]
19. Priel A, et al. Stargazin reduces desensitization and slows deactivation of the AMPA-type glutamate receptors. J Neurosci. 2005; 25:2682–2686. [PubMed: 15758178]
20. Tomita S, et al. Stargazin modulates AMPA receptor gating and trafficking by distinct domains. Nature. 2005; 435:1052–1058. [PubMed: 15858532]
21. Turetsky D, Garringer E, Patneau DK. Stargazin modulates native AMPA receptor functional properties by two distinct mechanisms. J Neurosci. 2005; 25:7438–7448. [PubMed: 16093395]
22. Bedoukian MA, Weeks AM, Partin KM. Different domains of the AMPA receptor direct stargazin-mediated trafficking and stargazin-mediated modulation of kinetics. J Biol Chem. 2006; 281:23908–23921. [PubMed: 16793768]
23. Cho CH, St-Gelais F, Zhang W, Tomita S, Howe JR. Two families of TARP isoforms that have distinct effects on the kinetic properties of AMPA receptors and synaptic currents. Neuron. 2007; 55:890–904. [PubMed: 17880893]

24. Kott S, Sager C, Tapken D, Werner M, Hollmann M. Comparative analysis of the pharmacology of GluR1 in complex with transmembrane AMPA receptor regulatory proteins gamma2, gamma3, gamma4, and gamma8. Neuroscience. 2009; 158:78–88. [PubMed: 18304748]
25. Tomita S, et al. Functional studies and distribution define a family of transmembrane AMPA receptor regulatory proteins. Journal of Cell Biology. 2003; 161:805–816. [PubMed: 12771129]
26. Kato AS, et al. New transmembrane AMPA receptor regulatory protein isoform, gamma-7, differentially regulates AMPA receptors. J Neurosci. 2007; 27:4969–4977. [PubMed: 17475805]
27. Soto D, et al. Selective regulation of long-form calcium-permeable AMPA receptors by an atypical TARP, gamma-5. Nat Neurosci. 2009; 12:277–285. [PubMed: 19234459]
28. Fukaya M, Yamazaki M, Sakimura K, Watanabe M. Spatial diversity in gene expression for VDCCgamma subunit family in developing and adult mouse brains. Neurosci Res. 2005; 53:376–383. [PubMed: 16171881]
29. Yamazaki M, et al. TARPs gamma-2 and gamma-7 are essential for AMPA receptor expression in the cerebellum. Eur J Neurosci. 2010; 31:2204–2220. [PubMed: 20529126]
30. Jackson AC, Nicoll RA. Stargazin (TARP gamma-2) is required for compartment-specific AMPA receptor trafficking and synaptic plasticity in cerebellar stellate cells. J Neurosci. 2011; 31:3939–3952. [PubMed: 21411637]
31. Bats C, Soto D, Studniarczyk D, Farrant M, Cull-Candy SG. Channel properties reveal differential expression of TARPed and TARPless AMPARs in *stargazer* neurons. Nat Neurosci. 2012; 15:853–861. [PubMed: 22581185]
32. Hashimoto K, et al. Impairment of AMPA receptor function in cerebellar granule cells of ataxic mutant mouse stargazer. J Neurosci. 1999; 19:6027–6036. [PubMed: 10407040]
33. Chen L, et al. Stargazin regulates synaptic targeting of AMPA receptors by two distinct mechanisms. Nature. 2000; 408:936–943. [PubMed: 11140673]
34. Bats C, Groc L, Choquet D. The interaction between Stargazin and PSD-95 regulates AMPA receptor surface trafficking. Neuron. 2007; 53:719–734. [PubMed: 17329211]
35. Gallo V, et al. Molecular cloning and development analysis of a new glutamate receptor subunit isoform in cerebellum. J Neurosci. 1992; 12:1010–1023. [PubMed: 1372042]
36. Mosbacher J, et al. A molecular determinant for submillisecond desensitization in glutamate receptors. Science. 1994; 266:1059–1062. [PubMed: 7973663]
37. Cathala L, Holderith NB, Nusser Z, DiGregorio DA, Cull-Candy SG. Changes in synaptic structure underlie the developmental speeding of AMPA receptor-mediated EPSCs. Nat Neurosci. 2005; 8:1310–1318. [PubMed: 16172604]
38. Schwenk J, et al. Functional proteomics identify cornichon proteins as auxiliary subunits of AMPA receptors. Science. 2009; 323:1313–1319. [PubMed: 19265014]
39. Shi Y, et al. Functional comparison of the effects of TARPs and cornichons on AMPA receptor trafficking and gating. Proceedings of the National Academy of Sciences of the United States of America. 2010; 107:16315–16319. [PubMed: 20805473]
40. Soto D, Coombs ID, Kelly L, Farrant M, Cull-Candy SG. Stargazin attenuates intracellular polyamine block of calcium-permeable AMPA receptors. Nat Neurosci. 2007; 10:1260–1267. [PubMed: 17873873]
41. Washburn MS, Dingledine R. Block of alpha-amino-3-hydroxy-5-methyl-4-isoxazolepropionic acid (AMPA) receptors by polyamines and polyamine toxins. J Pharmacol Exp Ther. 1996; 278:669–678. [PubMed: 8768718]
42. Koike M, Iino M, Ozawa S. Blocking effect of 1-naphthyl acetyl spermine on Ca^{2+}-permeable AMPA receptors in cultured rat hippocampal neurons. Neurosci Res. 1997; 29:27–36. [PubMed: 9293490]
43. Blaschke M, et al. A single amino acid determines the subunit-specific spider toxin block of alpha-amino-3-hydroxy-5-methylisoxazole-4-propionate/kainate receptor channels. Proceedings of the National Academy of Sciences of the United States of America. 1993; 90:6528–6532. [PubMed: 8393569]
44. Tomita S, Stein V, Stocker TJ, Nicoll RA, Bredt DS. Bidirectional synaptic plasticity regulated by phosphorylation of stargazin-like TARPs. Neuron. 2005; 45:269–277. [PubMed: 15664178]

45. Menuz K, O'Brien JL, Karmizadegan S, Bredt DS, Nicoll RA. TARP redundancy is critical for maintaining AMPA receptor function. J Neurosci. 2008; 28:8740–8746. [PubMed: 18753375]
46. Kato AS, Siuda ER, Nisenbaum ES, Bredt DS. AMPA receptor subunit-specific regulation by a distinct family of type II TARPs. Neuron. 2008; 59:986–996. [PubMed: 18817736]
47. Rouach N, et al. TARP gamma-8 controls hippocampal AMPA receptor number, distribution and synaptic plasticity. Nat Neurosci. 2005; 8:1525–1533. [PubMed: 16222232]
48. Shi Y, Lu W, Milstein AD, Nicoll RA. The stoichiometry of AMPA receptors and TARPs varies by neuronal cell type. Neuron. 2009; 62:633–640. [PubMed: 19524523]
49. Kim KS, Yan D, Tomita S. Assembly and stoichiometry of the AMPA receptor and transmembrane AMPA receptor regulatory protein complex. J Neurosci. 2010; 30:1064–1072. [PubMed: 20089915]
50. Yan D, Tomita S. Defined criteria for auxiliary subunits of glutamate receptors. J Physiol. 2012; 590:21–31. [PubMed: 21946847]
51. Letts VA, et al. The mouse stargazer gene encodes a neuronal Ca^{2+}-channel gamma subunit. Nat Genet. 1998; 19:340–347. [PubMed: 9697694]
52. Passafaro M, Nakagawa T, Sala C, Sheng M. Induction of dendritic spines by an extracellular domain of AMPA receptor subunit GluR2. Nature. 2003; 424:677–681. [PubMed: 12904794]
53. Schneider CA, Rasband WS, Eliceiri KW. NIH Image to ImageJ: 25 years of image analysis. Nat Methods. 2012; 9:671–675. [PubMed: 22930834]
54. Ferron L, et al. The stargazin-related protein gamma 7 interacts with the mRNA-binding protein heterogeneous nuclear ribonucleoprotein A2 and regulates the stability of specific mRNAs, including CaV2.2. J Neurosci. 2008; 28:10604–10617. [PubMed: 18923037]
55. Chung C, Deak F, Kavalali ET. Molecular substrates mediating lanthanide-evoked neurotransmitter release in central synapses. J Neurophysiol. 2008; 100:2089–2100. [PubMed: 18715899]
56. Kudoh SN, Taguchi T. A simple exploratory algorithm for the accurate and fast detection of spontaneous synaptic events. Biosens Bioelectron. 2002; 17:773–782. [PubMed: 12191925]
57. Traynelis SF, Silver RA, Cull-Candy SG. Estimated conductance of glutamate receptor channels activated during EPSCs at the cerebellar mossy fiber-granule cell synapse. Neuron. 1993; 11:279–289. [PubMed: 7688973]
58. Wilcox, RR. Introduction to robust estimation and hypothesis testing. Academic Press; Amsterdam ; Boston: 2012.
59. Maechler, M.; Rousseeuw, P.; Struyf, A.; Hubert, M.; Hornik, K. Cluster analysis basics and extensions. R package version 1.14.3. 2012.

Europe PMC Funders Author Manuscripts

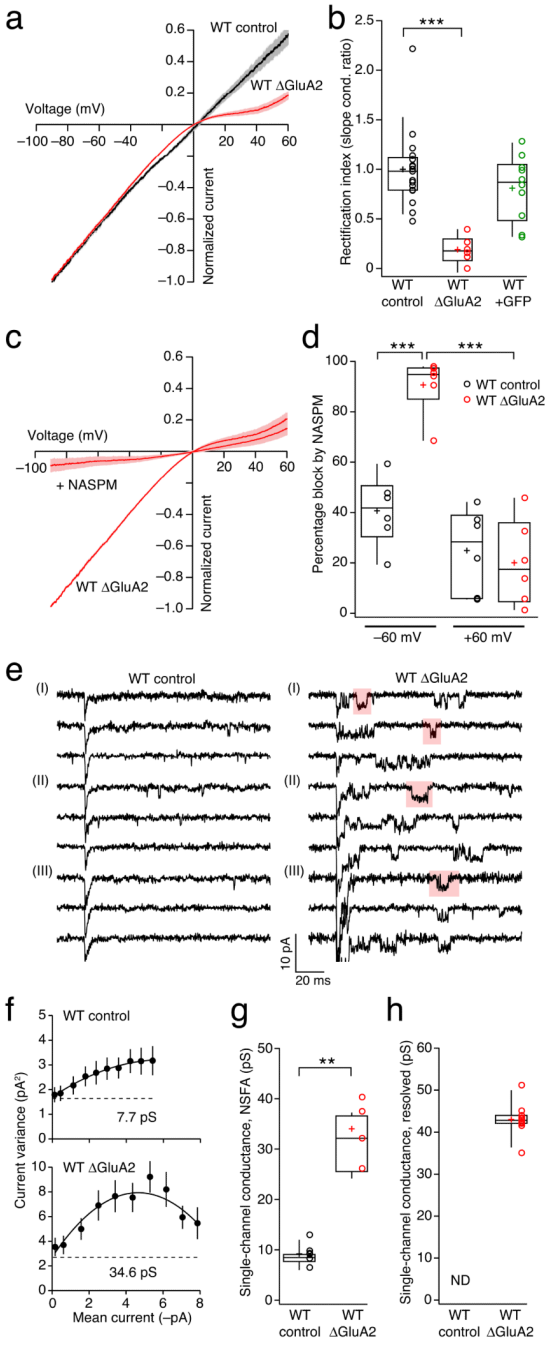

Figure 1.

GluA2 knockdown in cerebellar granule cells results in expression of CP-AMPARs. (**a**) Global average current-voltage relationships recorded from control (black, *n* =17) and ΔGluA2 cells (red, *n* = 6 cells) in response to 20 μM AMPA. Grey and pink shaded areas denote s.e.m. (**b**) Rectification index values for control, ΔGluA2, and GFP transfected cells (*n* = 10 cells). *** $P < 0.0001$. (**c**) Global average current-voltage relationships recorded from ΔGluA2 cells (*n* = 6 cells) before and after bath application of 100 μM NASPM. (**d**) Percentage block by NASPM at −60 and +60 mV in wild-type (*n* = 6 cells) and ΔGluA2 cells (*n* = 6 cells). *** $P < 0.0001$. (**e**) Representative macroscopic responses to 100 ms

Europe PMC Funders Author Manuscripts

application of 1 mM AMPA onto outside-out patches at −60 mV. Three individual responses from each of three different patches (I, II and III) are shown for wild-type and ΔGluA2 cells (traces are filtered at 2 kHz, for display). Long-lived bursts of openings (selected examples highlighted in red) were present in the tail of the macroscopic currents from ΔGluA2 patches; in wild-type patches openings were much briefer and less discernible (see **Methods**). (**f**) Representative current-variance plots from non-stationary fluctuation analysis. Symbols denote mean variance in each of ten equally spaced amplitude bins. Vertical error bars denote s.e.m. In each case, the weighted-mean single-channel current from the weighted parabolic fit to the data is shown. The dashed lines indicate the background current variance. (**g**) Pooled data showing a dramatic increase in single-channel conductance after GluA2 knockdown (n = 7 and 4 patches from wild-type and ΔGluA2 cells, respectively). ** $P < 0.01$. (**h**) Single-channel events were directly resolved in 11 of 12 patches from ΔGluA2 cells but in 0 of 18 patches from wild-type cells. In panels **b**, **d**, **g** and **h**, box-and-whisker plots indicate the median value (black line), the mean (cross), the 25-75th percentiles (box) and the 10-90th percentiles (whiskers); open circles show individual values.

Europe PMC Funders Author Manuscripts

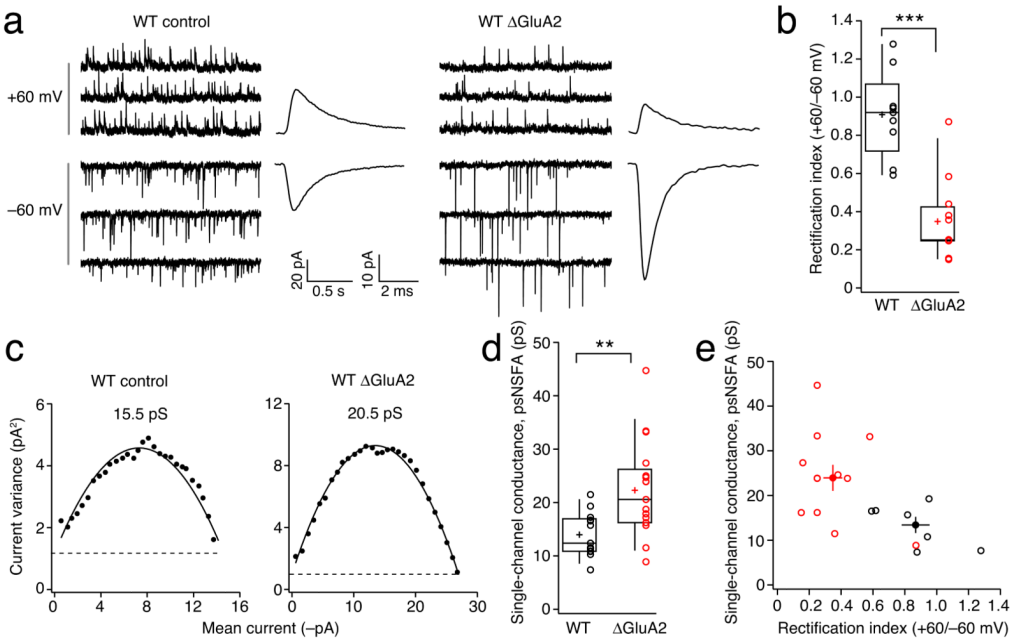

Figure 2.

CP-AMPARs mediate mEPSCs following GluA2 knockdown. (**a**) Representative AMPAR-mediated mEPSCs recorded at positive and negative membrane potentials from a WT control cell and a ΔGluA2 cell. Right hand panels show the corresponding mean events. (**b**) Pooled data showing a decrease in rectification index following GluA2 knockdown (n = 9 and 12 WT and ΔGluA2 cells, respectively; *** $P < 0.001$). (**c**) Representative current-variance plots from peak-scaled non-stationary fluctuation analysis. Symbols denote mean variance in each of 30 equally spaced amplitude bins. In each case, the weighted-mean single-channel current from the weighted parabolic fit to the data is shown. The dashed line indicates the background current variance. (**d**) Pooled data showing the increased synaptic single-channel conductance in ΔGluA2 compared to wild-type cells (n = 17 and 13 cells, respectively; ** $P = 0.01$). (**e**) Scatter plot illustrating the shift in single-channel conductance and rectification index following GluA2 knockdown. Open symbols denote individual cells and closed symbols indicate the corresponding mean values (error bars denote s.e.m.). In panels **b** and **d**, box-and-whisker plots indicate the median value (black line), the mean (cross), the 25-75th percentiles (box) and the 10-90th percentiles (whiskers); open circles show individual values.

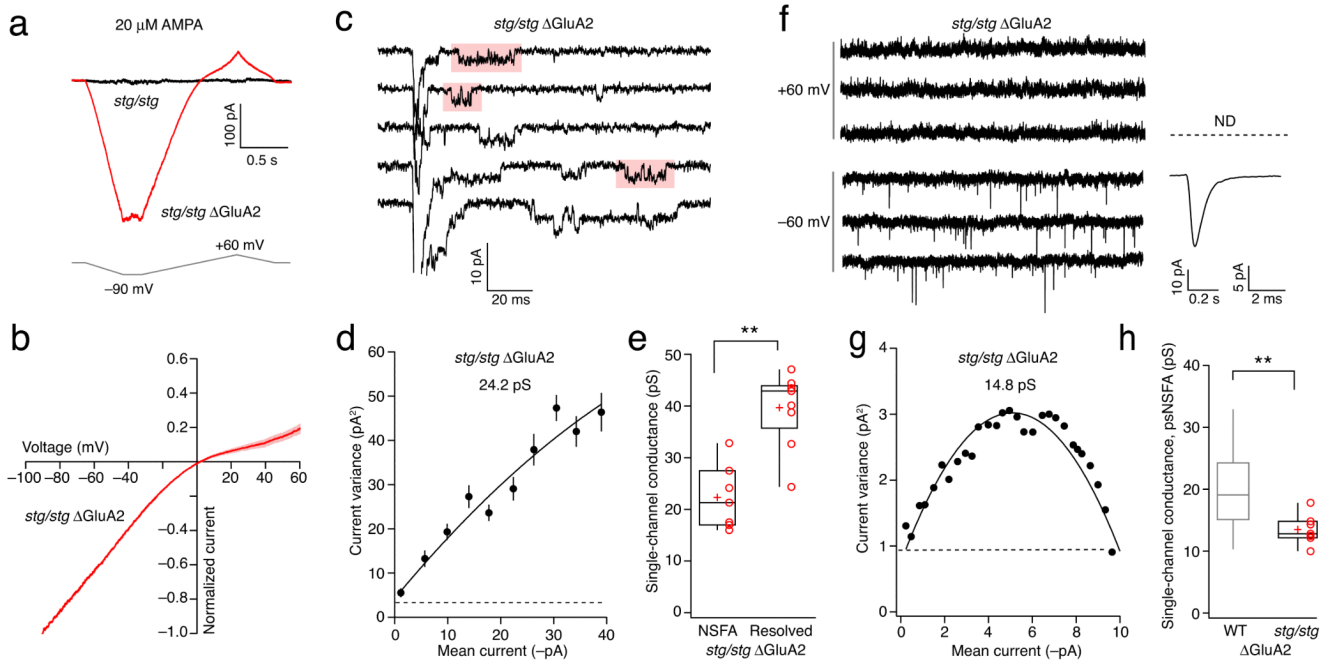

Figure 3.

CP-AMPARs are successfully trafficked to the cell surface in *stg/stg* cerebellar granule cells. (**a**) Representative whole-cell current records obtained in the presence of 20 μM AMPA during ramp changes in membrane voltage. The traces are from a *stg/stg* cell (black) and a *stg/stg* ΔGluA2 (red). Grey trace shows the voltage protocol. (**b**) Global average current-voltage relationship from *stg/stg* ΔGluA2 cells (n = 5 cells) showing marked inward rectification. Shaded area denotes s.e.m. (**c**) Representative macroscopic currents evoked by rapid application of 1 mM AMPA onto an outside-out patch from a *stg/stg* ΔGluA2 cell. Red highlights indicate selected examples of clear channel openings in the tail of the current. (**d**) Representative current-variance plot from non-stationary fluctuation analysis. Symbols denote mean variance in each of ten equally spaced amplitude bins. Vertical error bars denote s.e.m. The weighted-mean single-channel current from the parabolic fit to the data is shown. The dashed line indicates the background current variance. (**e**) Pooled data showing single-channel conductance estimates from NSFA and resolved channel openings (n = 7 and 9 patches, respectively from *stg/stg* ΔGluA2 cells). ** $P < 0.01$. (**f**) Representative mEPSCs recorded at +60 and −60 mV from a *stg/stg* cerebellar granule cell after GluA2 knockdown. Right-hand panel shows averaged event at −60 mV and absence of detected events at +60 mV. (**g**) Representative current-variance plot from peak-scaled non-stationary fluctuation analysis. Symbols denote mean variance in each of 30 equally spaced amplitude bins. The weighted-mean single-channel current from the parabolic fit to the data is shown. The dashed line indicates the background current variance. (**h**) Pooled data showing the decreased weighted mean single-channel conductance (from psNSFA) in *stg/stg* ΔGluA2 cells (n = 9 cells) compared to wild-type ΔGluA2 cells (grey box-and-whisker plot from Fig. 2d; ** $P < 0.01$). In panels **e** and **h**, box-and-whisker plots indicate the median value (black line), the mean (cross), the 25-75th percentiles (box) and the 10-90th percentiles (whiskers); open circles show individual values.

Europe PMC Funders Author Manuscripts

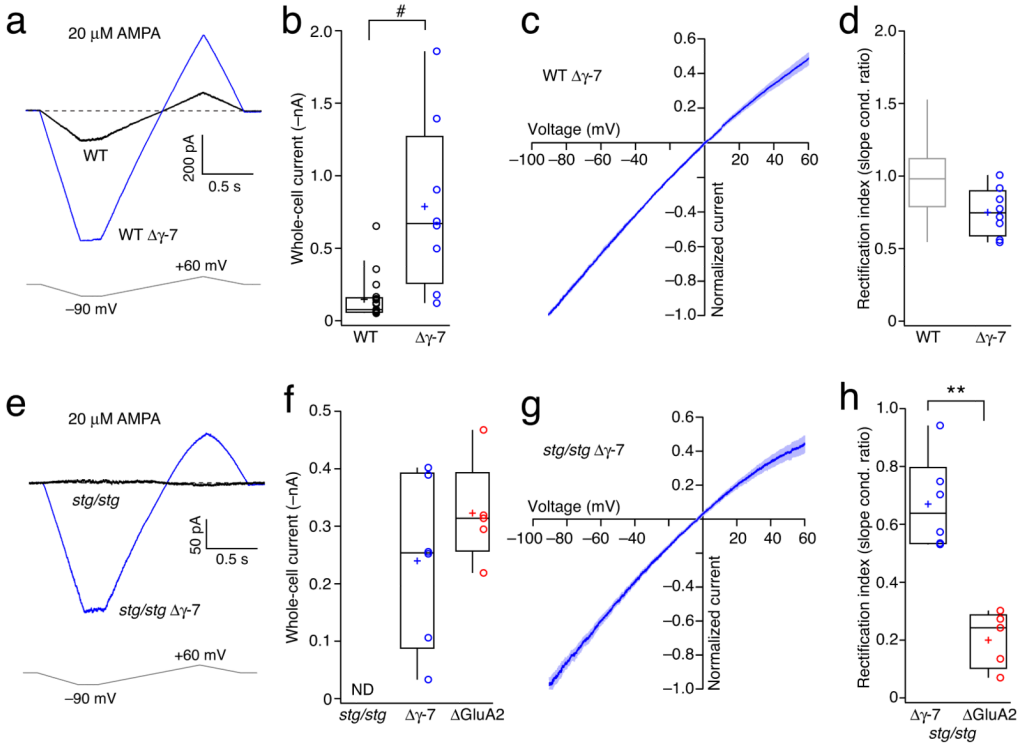

Figure 4.

Presence of γ-7 determines the level of surface expression of CI-AMPARs in wild-type and *stg/stg* cerebellar granule cells. (**a**) Representative whole-cell current records from a wild-type cell (black) and a Δγ-7 cell (blue) obtained in the presence of 20 μM AMPA during ramp changes in membrane voltage. Grey trace shows the voltage protocol. (**b**) Pooled data showing AMPA-evoked whole-cell current (−90 mV) following knockdown of γ-7 (n = 17 wild-type and 8 Δγ-7 cells; # P = 0.055 Welch t-test and $P < 0.05$ robust methods (see Supplementary Table 2). (**c**) Global average current-voltage relationship recorded from Δγ-7 cells (n = 8 cells) indicating a lack of rectification. Shaded area denotes s.e.m. (**d**) Pooled data showing that rectification index did not change following knockdown of γ-7 (n = 8 Δγ-7 cells). For comparison, the grey box-and-whisker plot for wild-type cells is from Fig. 1b. (**e-h**) Corresponding data showing the restoration of whole-cell currents following knockdown of γ-7 in *stg/stg* granule cells (n = 8 and 6 cells for *stg/stg* and *stg/stg* Δγ-7, respectively). In panel **f** and **h**, pooled data showing the whole-cell current and rectification index in *stg/stg* ΔGluA2 cells are shown for comparison (n = 5 cells; red). ** $P < 0.01$. In panels **b**, **d**, **f** and **h**, box-and-whisker plots indicate the median value (black line), the mean (cross), the 25-75th percentiles (box) and the 10-90th percentiles (whiskers); open circles show individual values.

Europe PMC Funders Author Manuscripts

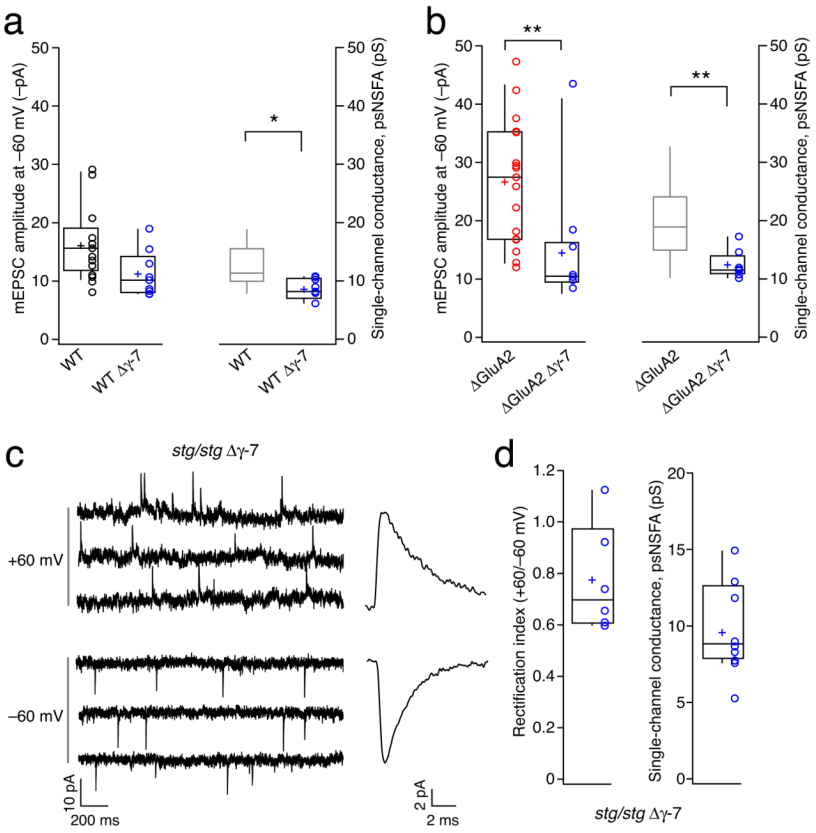

Figure 5.

Single and double knockdown experiments suggest a role of γ-7 in the regulation of synaptic AMPARs. (**a**) Pooled data illustrating the mEPSC amplitude at −60 mV (*n* = 12 and 9 cells) and reduction in synaptic single-channel conductance (*n* = 13 and 9 cells) following the knockdown of γ-7 in wild-type granule cells (CI-AMPARs). * *P* <0.05. The grey box-and-whisker plot for WT is from Fig. 2d. (**b**) Corresponding data showing the effect of γ-7 knockdown in WT ΔGluA2 granule cells *n* = 17 ΔGluA2 and 8 ΔGluA2Δγ-7 cells). ** *P* < 0.01. The grey box-and-whisker plot for WT ΔGluA2 cells is from Fig. 2d. (**c**) Representative mEPSCs recorded at +60 and −60 mV from a *stg/stg* cerebellar granule cell after knockdown of γ-7. Right-hand panel shows averaged events at the two potentials. (**d**) Pooled data showing rectification index and single-channel conductance for *stg/stg* Δγ-7 cells (*n* = 6 and 9 cells). In panels **a**, **b** and **d**, box-and-whisker plots indicate the median value (black line), the mean (cross), the 25-75th percentiles (box) and the 10-90th percentiles (whiskers); open circles show individual values.

Europe PMC Funders Author Manuscripts

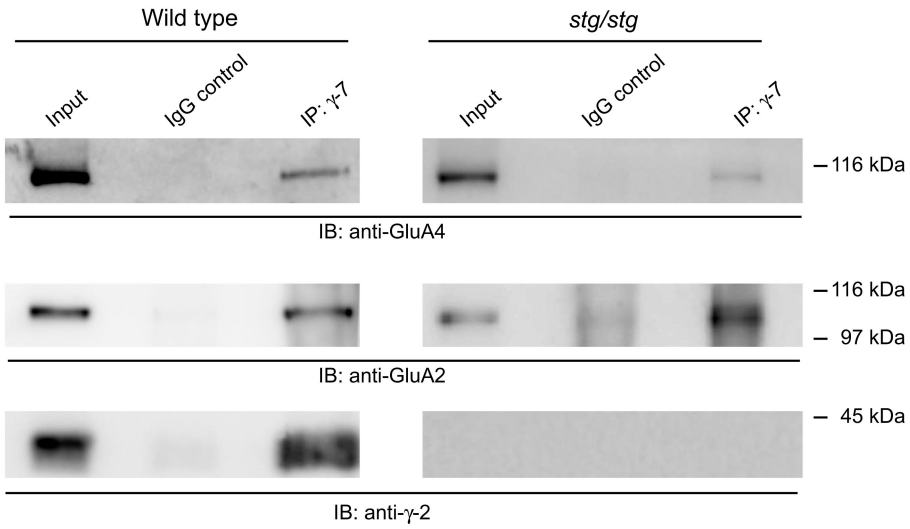

Figure 6.

AMPAR subunits GluA2 and GluA4 co-immunoprecipitate with TARP γ-7 in cerebellar lysates from both wild-type and *stg/stg* mice. γ-7 additionally co-immunoprecipitates with γ-2 in wild-type cerebellum. γ-7 protein complexes were immunoprecipitated (IP) with anti-γ-7 antibody then western blotted, along side input samples and IgG controls, using anti-GluA4, anti-GluA2 or anti- γ-2 antibodies (IB; immunoblot). Input fractions were 1.5% of the total, except for wild type GluA2 and γ-2 where they were 0.5%. In each case the nearest molecular weight markers are indicated. Each immunoblot illustrated is representative of 2-5 replicates.Illustrated blots are cropped; un-cropped blots are shown in Supplementary Figure 3.

Europe PMC Funders Author Manuscripts

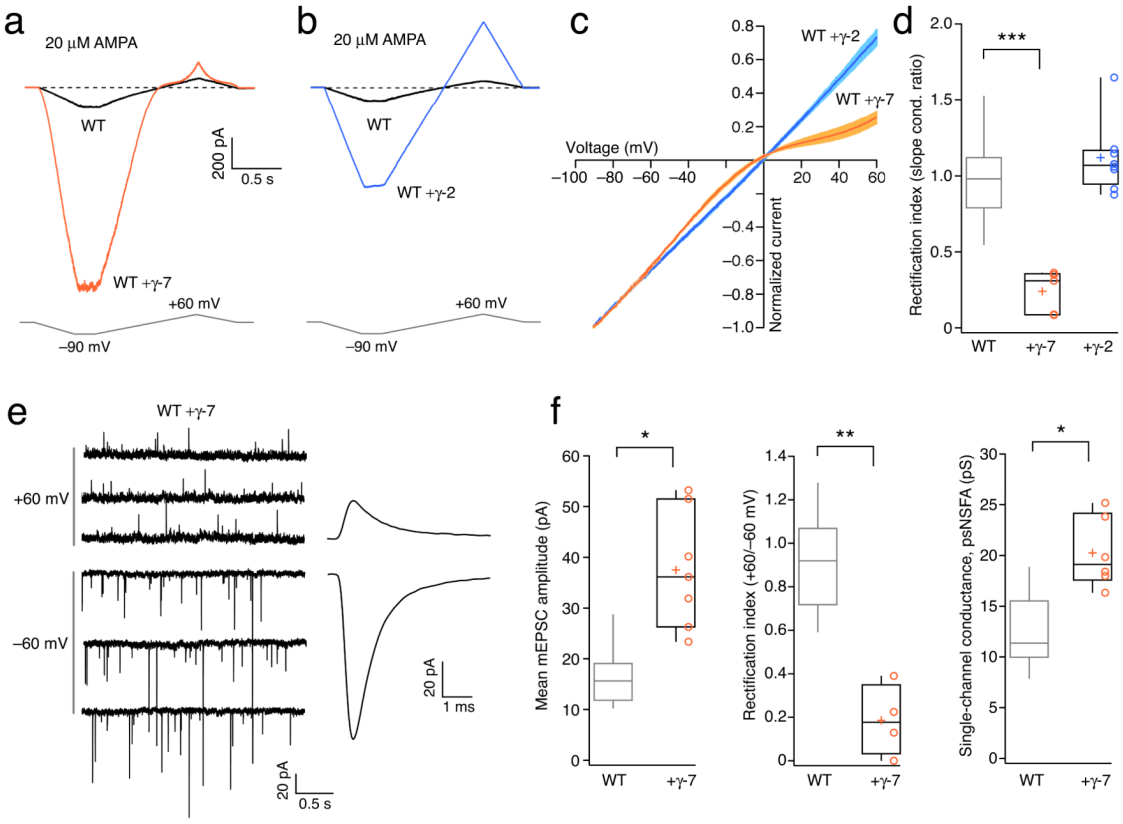

Figure 7.

Over-expression of γ-7 in cerebellar granule cells causes a switch from CI- to CP-AMPARs. (**a**) Representative whole-cell current records from a wild-type cell (black) and a +γ-7 cell (orange) obtained in the presence of 20 μM AMPA during ramp changes in membrane voltage. Grey trace shows the voltage protocol. (**b**) Representative records (as in **a**) showing the effect of over-expression of γ-2 (cyan). (**c**) Global average current-voltage relationships recorded from +γ-2 (cyan, $n = 8$) and +γ-7 cells (orange, $n = 5$). Shaded areas denote s.e.m. (**d**) Pooled data showing the effects of over-expression of γ-7 ($n = 5$ cells) and γ-2 ($n = 8$ cells) on rectification index. The grey box-and-whisker plot for wild-type cells is from Fig. 1b. *** $P < 0.001$. (**e**) Representative mEPSCs recorded at +60 and −60 mV from a wild-type cerebellar granule cell after over-expression of γ-7. Right-hand panel shows averaged events at the two potentials. (**f**) Pooled data showing changes in mEPSC amplitude, rectification index and single-channel conductance following over-expression of γ-7 ($n = 7$, 4 and 6 cells). For comparison, the grey box-and-whisker plots for wild-type cells are from Figs. 5a, 2b and 2d. * $P < 0.05$. ** $P < 0.01$. In panels **d** and **f**, box-and-whisker plots indicate the median value (black line), the mean (cross), the 25-75th percentiles (box) and the 10-90th percentiles (whiskers); open circles show individual values.

Europe PMC Funders Author Manuscripts